

An effective and smart corrosion inhibitor in acidic environment: Experimental & theoretical studies

Asmae Bouoidina^{*,‡}, Rajesh Haldhar^{**,‡}, Rajae Salim^{*,†}, Elhachmia Ech-chihbi^{*}, Hamza Ichou^{***},
Fadoua El-Hajjaji^{*}, Seong-Cheol Kim^{**,†}, Brahim El Ibrahimi^{****}, Savas Kaya^{*****}, and Mustapha Taleb^{*}

^{*}Engineering Laboratory of Organometallic, Molecular Materials, and Environment, Faculty of Sciences,
University Sidi Mohamed Ben Abdellah, Fez, Morocco

^{**}School of Chemical Engineering, Yeungnam University, Gyeongsan 38541, Korea

^{***}Centre d'élaboration de Matériaux et d'études Structurales, CEMES-CNRS, UPR 8011, F-31055 Toulouse, France

^{****}Applied Chemistry-Physic Team, Faculty of Sciences, University of Ibn Zohr, Agadir, Morocco

^{*****}Sivas Cumhuriyet University, Math. and Sci. Edu., 58140, Sivas, Turkey

(Received 31 March 2022 • Revised 15 June 2022 • Accepted 29 July 2022)

Abstract—The application of corrosion inhibitors is the best way to protect metals from degradation. Therefore, the P-anisidine molecule was investigated as a corrosion inhibitor for mild steel in a 1 M HCl medium. This study used different methods, such as electrochemical impedance spectroscopy, polarization potentiodynamic curves, scanning electron microscopy, and theoretical method. The addition of this molecule to the aggressive medium achieved inhibition of 81% at a concentration of 10^{-3} M. The potentiodynamic polarization curves reveal a mixed type character (anodic and cathodic) and adsorb on the metal surface according to Langmuir adsorption isotherm. This adsorption was also proved by scanning electron microscopy proving the presence of a protective layer on the steel surface used. The theoretical results confirmed the experimental part and showed that P-anisidine adsorbed parallel onto the steel surface covering a large surface area.

Keywords: P-anisidine, Mild Steel, Theoretical Calculation, Dynamic Simulation

INTRODUCTION

The serious effects of corrosion have turned into a major global problem, especially concerning the enormous economic cost of corrosion. The control of this phenomenon is obtained by understanding the corrosion mechanism using corrosion-resistant materials. In this context, mild steel is the most used due to its economic profitability and easy manufacture, but it remains sensitive to aggressive solutions. Hydrochloric acid is one of these acids which has many uses, especially in the acid pickling of steel [1,2]. The need to reduce the corrosion process necessitates the use of inhibitors, in particular organic compounds, which represent one of the simple means of fighting corrosion in acidic environments [3-5]. In general, heterogeneous organic compounds have a polar character caused by heteroatoms such as nitrogen, oxygen, and sulfur tending to resist corrosion; these compounds form strong coordination bonds with Fe atoms, which leads to the adsorption of species and the formation of a protective film on the metal surface [6,7].

Anisidine molecule is a simple molecule that contains two functions (aniline and methoxy) substituted with various methods by linking with ortho, meta, or para position. The P-anisidine compound can be defined also as 4-Methoxyaniline since containing

aniline function and methoxy motif substituted in the para position of the benzene ring. Also, it is mostly used for producing dyes, and texture processing. Also, it is employed for the synthesis of pharmaceuticals and liquid crystals by using a small quantity since having a high potential application [8,9]. It can be seen from the previous studies that anisole and aniline are widely used as corrosion inhibitors, which leads us to investigate also P-anisidine molecule. For example, Meenakshiet et al. [10] found that 5-chloro-2-nitroanisole showed a high inhibition efficiency based on DFT calculation, especially the maximum charge transfer and the back-donation values. In another study, Shukla et al. [11] indicated that linear copolymer of amines and formaldehyde showed a high inhibition performance for mild steel in HCl 1M based on various electrochemical techniques and analysis surface. Another compound (vinyl alcohol-omethoxy aniline) was investigated against corrosion of mild steel in HCl 1 M by Karthikaiselviet et al. [12], who confirmed the adsorption of the studied compound onto the steel surface, making a protective film barrier. In another medium, an improvement of the corrosion inhibition of electro-polymerized coatings based on aniline derivatives on copper in 0.5 M H_2SO_4 was performed by Yucong et al. [13] based on characterization and mechanism modeling.

In this work, the corrosion inhibition performance of the P-anisidine molecule (Fig. 1) molecule was examined using electrochemical methods like potentiodynamic polarization measurements and electrochemical impedance spectroscopy (EIS). However, these techniques do not allow exploration of the real inhibition mechanism

[‡]To whom correspondence should be addressed.

E-mail: salimrajae@gmail.com, sckim07@ynu.ac.kr

^{*}These authors contributed equally to this work.

Copyright by The Korean Institute of Chemical Engineers.

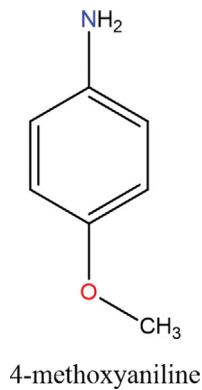


Fig. 1. Structure of P-anisidine molecule.

at the interface of the metal solution. For this, we resorted to theoretical techniques: the theory of functional density (DFT) and the simulation of molecular dynamics (MD) that are the most reliable to determine the correlation between the molecular properties of the inhibitors and their corresponding efficiencies.

EXPERIMENTAL

1. Material and Corrosive Medium

The mild steel used in the current work has the following composition: 0.01% Al, 0.05% Mn, 0.38% Si, 0.2% C, 0.09% P, 0.05% S, and the rest of the Fe. The corrosive solution is a solution of molar hydrochloric acid (HCl 1 M), obtained by diluting, with double distilled water, and concentrated commercial acid to 37%, noting that the studied compound is completely soluble in this medium. Before conducting the test, the specimens were polished with emery gradually paper, washed with distilled water, and degreased with acetone solvent.

2. Electrochemical Measurements

For all stationary ($i=f(E)$) and non-stationary (SIE) electrochemical measurements, we used an experimental device consisting of a potentiostat associated with the Voltalab software and connected to a conventional cell with three electrodes: A platinum electrode as an auxiliary electrode, a saturated calomel Hg/Hg₂Cl₂/KCl (ECS) electrode as the reference electrode and steel as the working electrode. Impedance measurements were made between 100 kHz and 100 mHz using an amplitude of 10 mV. For the polarization measurements, the potential was applied in a range between -600 and -200 mV relative to the corrosion potential with a scanning speed of 1 mVs⁻¹, and after a stabilization time of 30 minutes, this time was considered sufficient to reach a stable value of open circuit potential.

3. Analysis of Corroded Surfaces

SEM is currently the most widely used technique for topography at the microscopic scale. Its considerable advantage over optical microscopes, for example, is that the image does not suffer from a limited depth of field (FEI Company Quanta 200).

4. DFT Calculations

All calculations were performed with Gaussian 09 and GaussView5.0.8 software using the DFT method at the B3-LYP level with the basic set of 6-31G [14]. The following quantum parameters have been determined: E_{HOMO} , (E_{LUMO}), energy gap (ΔE_{gap}), global

hardness (η), global softness (σ), electronegativity (χ), dipole moment (μ), the fraction of electrons transferred (ΔN_{110}) using several equations [15,16]:

$$\Delta E_{gap} = E_{LUMO} - E_{HOMO} \quad (1)$$

$$\sigma = \frac{1}{\eta} \quad (2)$$

$$\eta = \frac{1}{2}(E_{HOMO} - E_{LUMO}) \quad (3)$$

$$\chi = \frac{1}{2}(E_{HOMO} + E_{LUMO}) \quad (4)$$

$$\Delta N_{110} = \frac{\chi_{Fe(110)} - \chi_{inh}}{2(\eta_{Fe(110)} + \eta_{inh})} = \frac{\Phi - \chi_{inh}}{2\eta_{inh}} \quad (5)$$

The chemical reactivity of the various atom of the molecule was determined by the Fukui indices, which are defined by the function of Fukui f_k corresponding to the site k of a molecule. These Fukui functions were used to compare reactive atomic centers within the same molecule. It can be calculated according to Eqs. (6) and (7):

$$P_k^- = P_k(N) - P_k(N-1) \quad \text{Electrophilic attack} \quad (6)$$

$$P_k^+ = P_k(N+1) - P_k(N) \quad \text{Nucleophilic attack} \quad (7)$$

where $P_k(N)$, $P_k(N+1)$, and $P_k(N-1)$ are the electronic population of the atom k in the neutral, anionic, and cationic forms, respectively [17,18].

5. Molecular Dynamic Simulations Study

MD simulation study is an interesting technique that can provide us with more details about the interfacial interactions between the steel surface and studied structure compounds. Therefore, the present investigation was conducted in the aqueous phase (100 H₂O, 3 H₃O⁺, and 3 Cl⁻), and a steel surface Fe(110) [19]. On the other hand, since the experimental study was evaluated in an acidic medium (i.e., 1 M HCl), the valuable protonated form of the tested molecule was taken into consideration. The COMPASS force field was performed to compute all energetic components, while Ewald and atom-based summation methods were used to evaluate the electrostatic and van der Waals non-bonding 699 interactions, respectively [20]. The simulations were performed in a box (17 Å×17 Å×74 Å) that includes eight layers of Fe(110) with 8×8 atoms per face and a vacuum region of 70 Å [21]. The total time of simulation was fixed at 100 ps with 1 fs as a time step at 298 K via the Anderson thermostat. The adsorption energy (E_{ads}) of the tested inhibitor was estimated according to Eq. (8):

$$E_{ads} = E_{total} - (E_{surface+solution} + E_{inhibitor}) \quad (8)$$

E_{total} , $E_{inhibitor}$ and $E_{surface+solution}$ represent the energy of the whole system, inhibitor molecule, and surface+solution, respectively [22,23].

RESULTS AND DISCUSSION

1. Open Circuit Potential (OCP)

The variation of the mild steel potential versus the time during 30 min for the uninhibited and the inhibited solution of P-anisidine

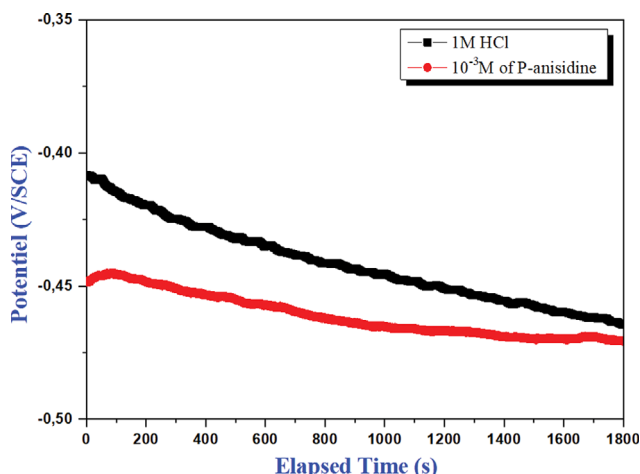


Fig. 2. OCP for mild steel in 1 M HCl at an optimum concentration of P-anisidine.

is presented in Fig. 2. The addition of the studied molecules reduces the corrosion potential E_{corr} . Based on these plots, it can be observed that the mild steel samples could achieve a quasi-stable open circuit potential during 30 min.

2. Polarization Curves

The Tafel lines of the anodic and cathodic curves have been to achieve the corrosion parameters such as the corrosion potential (E_{corr}), the corrosion current density (i_{corr}), the polarization resistance (R_p), the cathode slope of Tafel (β_c), respectively. The measured corrosion current densities in the absence of P-anisidine (i_0) and in its presence (i) were used to calculate the percentage of inhibitory efficiency using Eq. (9) [24]:

$$IE\% = [i_0 - i/i_0] \times 100 \quad (9)$$

The curves and the parameters obtained are shown in Fig. 3 and Table 1.

It appears from the first view of the polarization curves (Fig. 3) that the cathode lines of Tafel are in the form of parallel lines; this suggests that adding P-anisidine to the HCl solution does not modify the mechanism of evolution of the hydrogen and that the reduction of proton H^+ at the surface of mild steel mainly occurs through a charge transfer mechanism [25,26]. Therefore, this reduction can be performed by providing coverage of the active reaction sites of the steel under study. In addition, the values obtained for the cathodic slope (β_c) do not show a big difference with the increase of P-anisidine concentration, signifying that the reduction of hydrogen

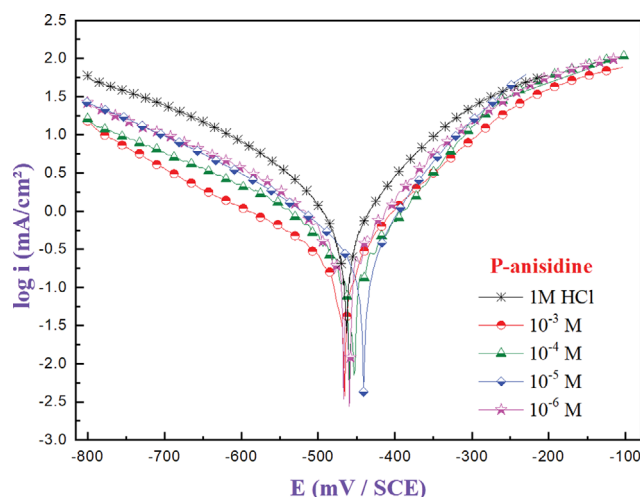


Fig. 3. Polarization curves of mild steel obtained at different concentrations of P-anisidine.

reaction is performed by pure activation mechanism [27].

It is known from the previous work that the inhibitors can be classified as cathodic or anodic when the potential displacement is more than 85 mV. If not, they act as mixed-type ones [28]. The data in the table clearly show that displacement of corrosion potential compared with blank remains lower than 85 mV, which means that P-anisidine is a mixed type of inhibitor. On the other hand, the density of the corrosion current decreases as a function of the concentration, contrary to the inhibitory efficiency, which is relative to the quantity of inhibitor adsorbed and which reaches a maximum of 81% at 10^{-3} M.

3. Impedance Measurements

The curves from the Nyquist and Bode plan are represented in Fig. 4, on which we note the presence of a single semicircular loop, whose size increases with the increase in the concentration of P-anisidine, due to the progressive formation of a protective film on the surface of the electrode. This electrochemical behavior shows that the corrosion process is controlled by the charge transfer phenomenon [29], the thing that we can confirm through the Bode diagrams by the presence of a single time constant for different concentrations of the inhibitor [30].

Both representations of impedance diagrams (Nyquist and Bode) were analyzed by an adjustment of the experimental data through the equivalent circuit model revealed in Fig. 5. Generally, due to the heterogeneity of the electrode surface, the capacitive loops are not perfect semicircles; therefore, we have introduced a constant

Table 1. Electrochemical parameters of corrosion in 1 M HCl in the absence and the presence of P-anisidine

Medium	C (M)	$-E_{corr}$ (mV/SCE)	i_{corr} (mA/cm ²)	$-\beta_c$ (mV dec ⁻¹)	R_p ($\Omega \cdot \text{cm}^2$)	IE (%)	SD
1 M HCl	**	464	1.258	171	34.7	-	0.0001
P-anisidine	10^{-3}	470	0.240	197	113.8	81.0	0.0004
	10^{-4}	458	0.257	139	110.6	79.6	0.0002
	10^{-5}	444	0.314	157	77.7	75.0	0.0006
	10^{-6}	453	0.350	138	87.1	72.2	0.0004

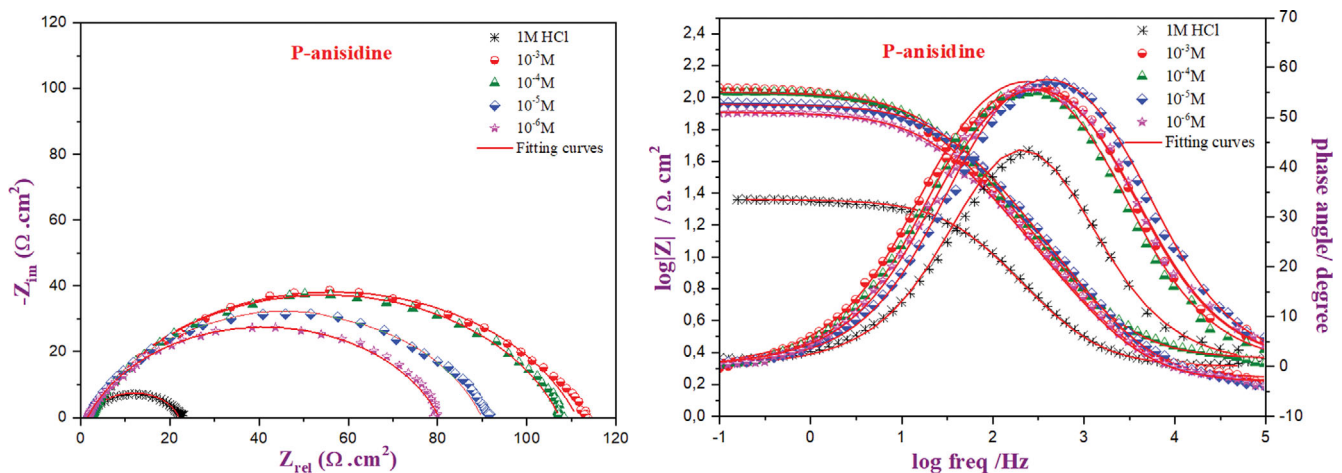


Fig. 4. Nyquist and Bode representation for P-anisidine compound.

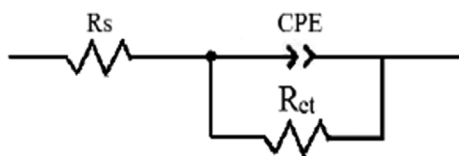


Fig. 5. Equivalent electrical circuit used for simulation.

phase element CPE defined by Eq. (10) [31].

$$Z_{CPE} = Q^{-1}(i\omega)^{-n} \tag{10}$$

where Q is a relative coefficient, n is linked to the phase shift and ω is the angular frequency ($\omega = 2\pi f_{max}$ with f_{max} is the maximum frequency).

The main adjusted parameters and inhibitory efficiency calculated from Eq. (11) [32] are given in Table 2.

$$E_{imp}(\%) = \frac{R - R_0}{R} \times 100 \tag{11}$$

where R_0 and R represent, respectively, the charge transfer resistance before and after the addition of P-anisidine.

First, a good agreement was detected between the experimental values and the calculated values of R_{ct} and E%, which justifies the satisfactory adjustment of the experimental spectra and that adjusted by the obtained circuit.

From Table 2, we observe that the charge transfer resistance increases and achieves a maximum of $108 \Omega \cdot \text{cm}^2$ at a concentration

of 10^{-3} M, which leads to a best inhibitory efficiency (81%). Also, the increase in the value of n compared to that obtained in the blank seems to be explained by a certain decrease in the heterogeneity of the surface, due to the adsorption of P-anisidine inhibitor on the most active sites of adsorption [33]. While the reduction in C_{dl} with the enhancement of P-anisidine concentration can be explained by the gradual replacement of the molecules on the metal surface, thus leading to the formation of a barrier film [34]. This decrease goes also with the same trend with the constant phase element Q obtained for the P-anisidine inhibitor. The decrease in this parameter with increasing concentration reflects an extension of a reduction in the local dielectric constant or the thickness of the double layer. Finally, good agreement was noted between the experimental values of R_{ct} and E% and those calculated from the curves adjusted by the CPE used, as well as the C_{dl} , which confirms the good choice of the studied model.

4. Adsorption Isotherm

Adsorption isotherms are often used to demonstrate the performance of the inhibitor and to determine the nature of the inhibitor/metal interaction. In this work, the data were experienced graphically adapting different isotherms (Freundlich, Temkin, Frumkin, Langmuir). Fig. 6 illustrates the various isotherm models traced for P-anisidine inhibitor based on electrochemical spectroscopy impedance analysis. The adsorption parameters of P-anisidine in HCl 1 M are collected in Table 3.

Langmuir isotherm
$$\frac{C_{inh}}{\theta} = \frac{1}{K} + C_{inh} \tag{12}$$

Table 2. Electrochemical parameters calculated after the adjustment of the P-anisidine diagram

Medium	C (M)	Rs ($\Omega \cdot \text{cm}^2$)	R_{ct}/Exp ($\Omega \cdot \text{cm}^2$)	R_{ct}/Fit ($\Omega \cdot \text{cm}^2$)	Q ($\mu\text{F s}^{n-1} \text{cm}^{-2}$)	n	C_{dl} ($\mu\text{F cm}^{-2}$)	E_{exp} (%)	E_{fit} (%)	θ
1 M HCl	-	2.0	22.0	20.6	483.0	0.806	160.0	-	-	-
P-anisidine	10^{-3}	2.2	108.2	108.0	146.3	0.768	42.0	79.7	80.8	0.808
	10^{-4}	2.1	102.1	98.4	149.3	0.800	52.2	78.5	78.9	0.789
	10^{-5}	1.4	92.1	90.5	215.6	0.750	58.2	76.1	77.1	0.771
	10^{-6}	1.8	79.0	79.4	277.9	0.770	89.5	72.2	73.9	0.739

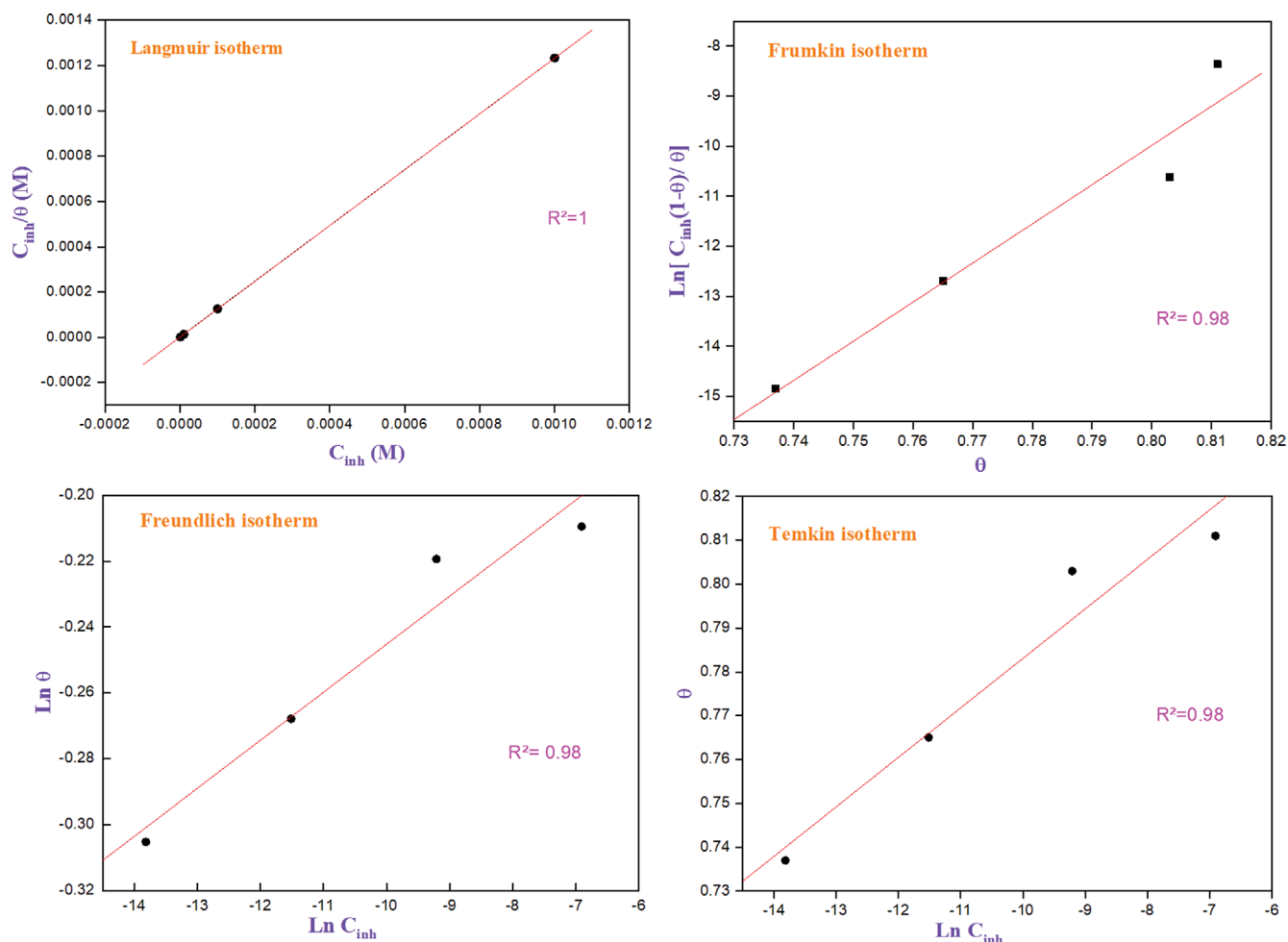


Fig. 6. Adsorption isotherm models of mild steel in 1 M HCl for P-anisidine.

Table 3. Adsorption parameters of P-anisidine in an acid medium

Isotherms	Parameters	R ²	K _{ads} (L mol ⁻¹)	ΔG _{ads} (Kj mol ⁻¹)	
Langmuir	Slope	1.23	1	8.27 10 ⁵	-43.7
Temkin	a	-51.18	0.98	1.07 10 ³⁹	-240.60
Frumkin	a	-47.24	0.98	8.33 10 ³⁶	-228.14
Freundlich	n	0.013	0.98	9.85 10 ⁻¹	-10.25

$$\text{Freundlich isotherm} \quad \ln \theta = \ln K + \frac{1}{n} \ln C_{inh} \quad (13)$$

$$\text{Frumkin isotherm} \quad \ln \left(\frac{C_{inh}(1-\theta)}{\theta} \right) = -\ln K - 2a\theta \quad (14)$$

$$\text{Temkin isotherm} \quad \theta = \frac{-1}{2a} \ln(K) - \frac{1}{2a} \ln(C_{inh}) \quad (15)$$

where C_{inh} : the inhibitor concentration; θ : the degree of surface coverage; a : the molecular lateral interactions; K : the equilibrium constant.

After determining the nature of the adsorption isotherm, we calculated the thermodynamic parameters, knowing that the equilib-

rium constant K_{ads} is related to the standard free energy of adsorption (ΔG_{ads}^0) by Eq. (16) [35]:

$$\Delta G_{ads}^0 = -RT \times \ln(55.5 \times K_{ads}) \quad (16)$$

Among the isotherms evaluated, the Langmuir isotherm seems to provide the best description of the absorption behavior of P-anisidine. From Fig. 6 we note that the curve $C_{inh}/\theta = f(C_{inh})$ is a straight line and the regression coefficient $R^2=1$ shows that the adsorption process obeys the Langmuir isotherm model. Also, the high value of K_{ads} is linked to the strong adsorption of the inhibitor, confirming the high adsorption of P-anisidine molecules [36]. Based on Freundlich isotherm analysis, it is clear that the small values obtained for the adsorption constant do not show a signification despite the high regression coefficient (0.98). In addition, the regression coefficient in Temkin and Frumkin isotherms is smaller than that obtained for Langmuir isotherm, which leads us to say that P-anisidine does not follow these two models. These results were confirmed since the experimental data are not close enough to the fitting curves in Temkin, Frumkin, and Freundlich models compared with the Langmuir [37,38].

Literally, the inhibitors can be making a chemical strong bond when the values of ΔG_{ads}^0 are around or more than -40 KJ mol^{-1} ,

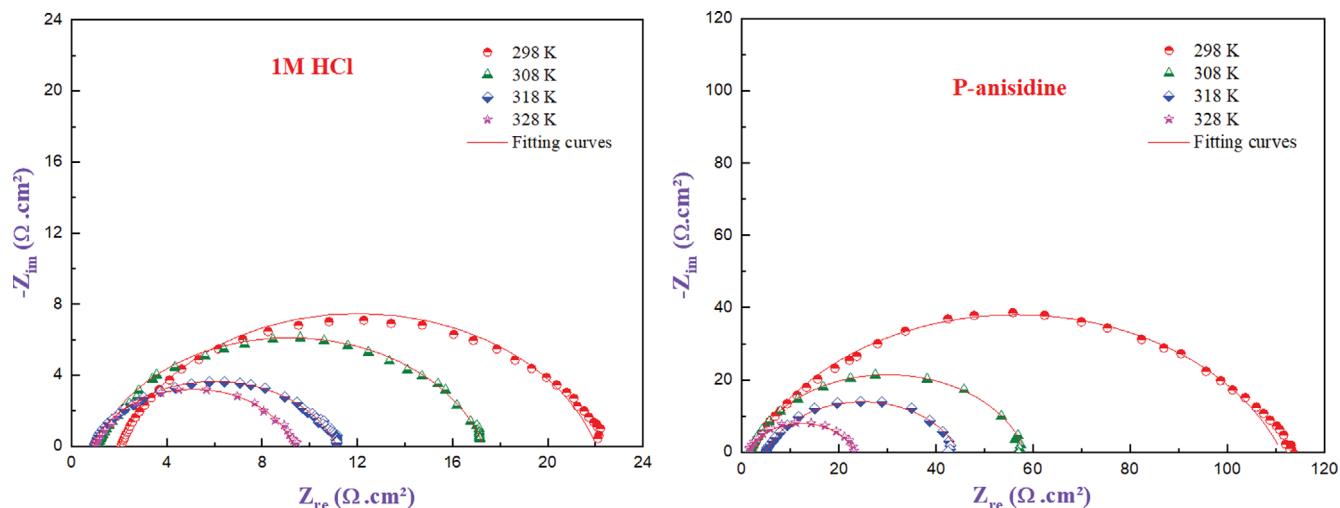


Fig. 7. Simulated Nyquist curves of P-anisidine data at various temperatures.

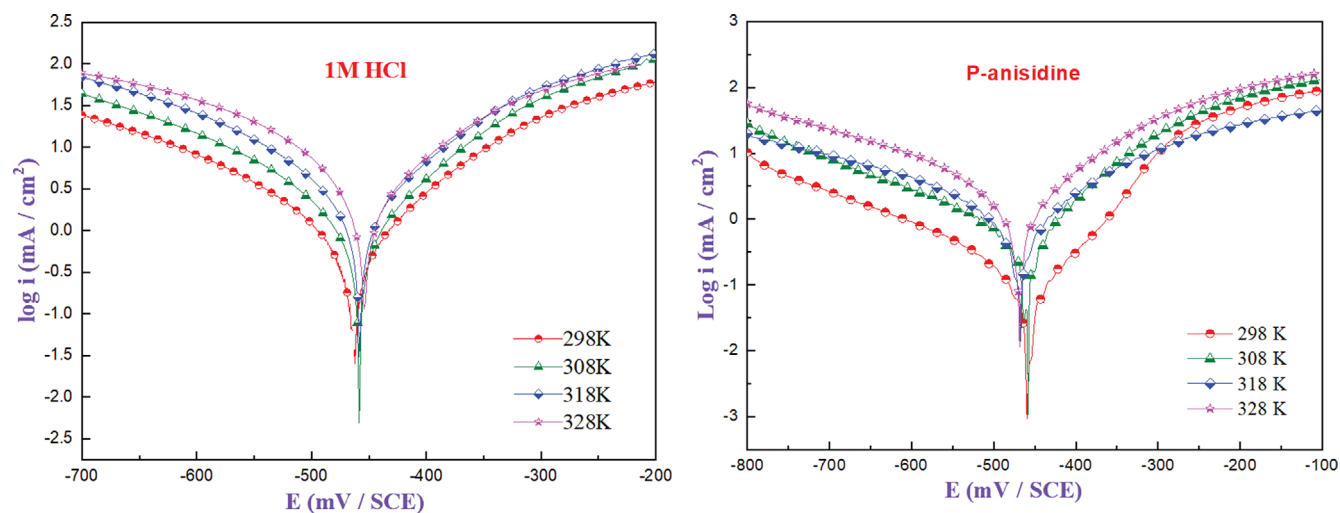


Fig. 8. Polarization curves without and with P-anisidine (10^{-3} M) at various temperatures.

Table 4. EIS and PDP parameters at different temperatures

T (K)	1 M HCl		P-anisidine			
	PDP	EIS	PDP		EIS	
	i_{corr} (mA cm $^{-2}$)	R_{ct} (Ω cm 2)	i_{corr} (mA cm $^{-2}$)	E_p (%)	R_{ct} (Ω cm 2)	E_{imp} (%)
298	1.258	23.0	0.240	80.9	108.0	80.8
308	2.179	18.1	0.609	72.1	55.4	71.8
318	3.331	11.7	1.026	69.2	41.71	61.2
328	4.479	9.8	2.027	54.7	21.48	54.2

while electrostatic bonds can be formed if ΔG_{ads}^0 are around -20 KJ mol $^{-1}$. In our case, the negative value of ΔG_{ads}^0 and which is in the vicinity of -40 kJ mol $^{-1}$ reflects, on the one hand, the spontaneity of the adsorption process and on the other, the formation of chemical bonds between the inhibitor and the metal surface [39].

5. Temperature effect

Fig. 7 and Fig. 8 present the impedance and polarization dia-

grams plotted at different temperatures in a 1 M HCl solution in the absence and the presence of 10^{-3} M of P-anisidine. The values of the parameters obtained by the different electrochemical methods at different temperatures (298-328 K) are summarized in Table 4.

The results obtained make it possible to deduce a clear decrease in the values of R_{ct} from the first increase in temperature from 298 K to 308 K. Their resistance was decreased from 108Ω cm 2 to

21.4 $\Omega \text{ cm}^2$. On the other hand, the PDP technique indicates that the corrosion current density increases with the increase of temperature, which implies a diminishment in the inhibition efficiency, confirming the EIS measurements. This decrease in IE% indicates that the increase in temperature causes desorption of P-anisidine from the steel surface. Consequently, it can be reported that the use of the P-anisidine inhibitor is ineffective at high temperatures. Based on electrochemical parameters of both inhibited and uninhibited medium, the obtained values show that the dissolution of the metal after the addition of our inhibitor is slower compared to the blank solution alone.

Many authors [40,41] use the Arrhenius equation and the transition state equation to account for the temperature effect on the density of the corrosion current i_{corr} and therefore consider that the logarithm $\ln i_{corr}$ and $\ln(i/T)$ are a linear function of the temperature inverse ($1,000/T$):

$$i_{corr} = A e^{\left(-\frac{E_a}{RT}\right)} \quad (17)$$

$$i_{corr} = \frac{RT}{Nh} \exp\left(\frac{\Delta S^*}{R}\right) \exp\left(-\frac{\Delta H^*}{RT}\right) \quad (18)$$

In these relations, E_a , ΔS^* , and ΔH^* represent the energy, entropy, and enthalpy of activation, k the pre-exponential parameter of Arrhenius, R constant of perfect gases ($8.314 \text{ J}\cdot\text{mol}^{-1}\cdot\text{K}^{-1}$), h Planck constant, N Avogadro's number, and T temperature in Kelvin. We plotted the variation of the logarithm of the density of the corrosion current at different temperatures as a function of the inverse of the absolute temperature T (Fig. 9). Table 5 presents the calculated activation parameters.

In literature, several researchers reported that inhibitors can be classified based on the evaluation of activation energy acquired in the nonappearance and the appearance of the inhibitor [42,43]. In the present study, the activation energy is greater in the existence of the inhibitor, which indicates that physical adsorption occurs.

In addition, the value of ΔH^* found is positive, which verifies the endothermic nature of the corrosion procedure. Thus, the value of the adsorption entropy is negative; this is attributed to a decrease

Table 5. Activation parameters for mild steel in 1 M HCl with and without 10^{-3} M of P-anisidine

Medium	E_a (KJ mol ⁻¹)	ΔH^* (KJ mol ⁻¹)	ΔS^* (J K ⁻¹ mol ⁻¹)
1 M HCl	33.9	31.9	-147.48
P-anisidine	55.4	53.8	-87.8

in the disorder which is due to the desorption of several molecules of water from the surface of the metal by the adsorption of a single molecule of the inhibitor [43,44].

6. Surface Analysis

To characterize and identify the surface of the metal with and without inhibitor, we used the SEM technique. Fig. 10(a) shows the morphology of the steel sample before immersion in the acid solution. Fig. 10(b) shows the surface of the steel after immersion in the acid solution. Fig. 10(c) shows the images of mild steel in the presence of an optimal concentration. It is clear from Fig. 10(a) that the surface of mild steel is very smooth and does not show any corrosion, just a few scratches due to the polishing of the metal by the abrasive paper. Unlike Fig. 10(b) which shows a rough and highly porous surface resulting from a corrosion attack. While in the presence of P-anisidine as shown in Fig. 10(c), the sample is much less damaged and has a smooth surface due to the formation of a protective layer of P-anisidine. This indicates that inhibiting corrosion prevents the dissolution of iron by reducing the rate of corrosion of mild steel in the 1 M HCl solution.

7. The Theoretical Approach to P-anisidine

7-1. Distribution of Electronic Density

To explain the adsorption of P-anisidine molecules on the surface of the steel, in a 1 M HCl solution, we undertook a theoretical study by the DFT method at the B3LYP/6-31G level, starting with optimization of the geometry and distribution of the HOMO and LUMO frontier orbitals of the protonated and neutral form of the molecule (Fig. 11).

The analysis of frontier molecular orbitals gives us important clues in terms of predicting the chemical reactivity of molecules.

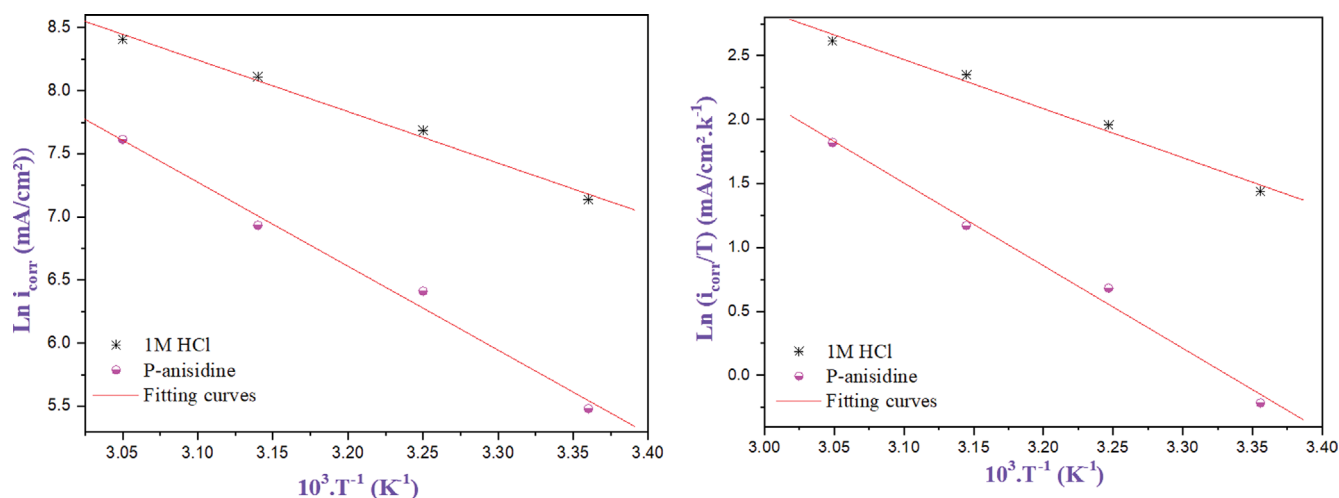


Fig. 9. $\ln(i_{corr})$ and $\ln(i_{corr}/T)$ versus $10^3/T$ with and without the addition of optimum concentration of P-anisidine.

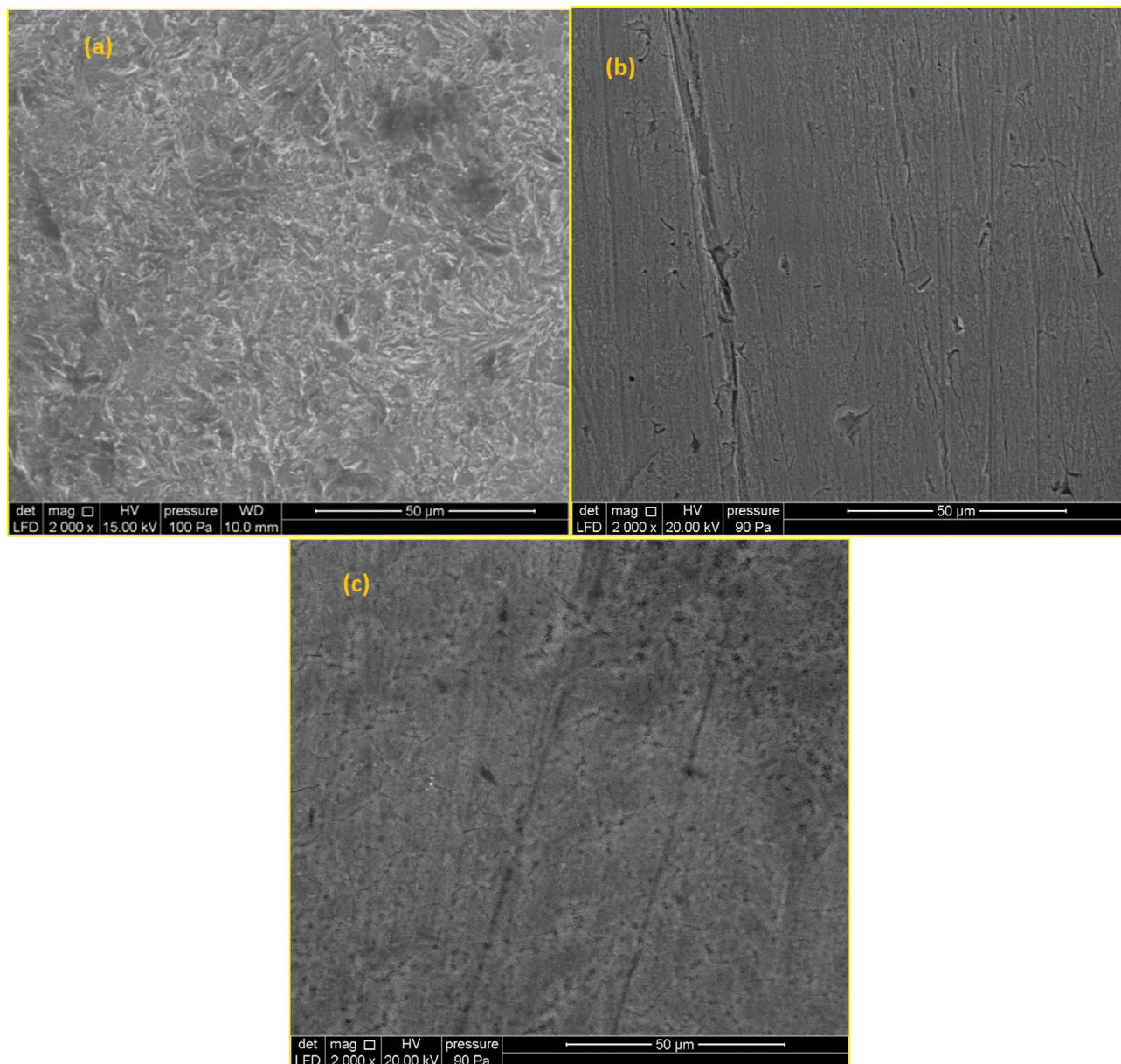


Fig. 10. SEM micrographs of the steel surface (a) before immersion; (b) after immersion in 1 M HCl; (c) in the presence of P-anisidine.

Table 6. Electronic parameters deduced by DFT at B3LYP/6-31 G (d, p) level for the neutral (N) and protonated (P) form of P-anisidine in the aqueous phase

Inhibitor	Form	E_{HOMO} (eV)	E_{LUMO} (eV)	ΔE (eV)	μ (D)	χ (eV)	η (eV)	σ (eV)	ΔN_{110} (eV)	E (%)
P-anisidine	N	-5.438	-0.074	5.363	3.551	2.756	2.681	0.372	0.384	≈81
	P	-6.632	-0.796	5.846	12.564	3.719	2.923	0.342	0.188	

From Fig. 11, we can notice that for neutral and protonated forms, the electronic density of LUMO is centered on the benzene nucleus. Otherwise, the HOMO density is found on the entire molecule, which shows that the adsorption will probably be done on several sites around the aromatic cycle and the atoms of oxygen and nitrogen. This result gives P-anisidine better inhibitory efficacy. Quantum parameters that have been calculated for P-anisidine in the

aqueous form are grouped in Table 6.

Generally, a high value of the HOMO energy facilitates the tendency of the molecule to yield electrons to species accepting electrons and having unoccupied molecular orbitals whose energy level is low and, consequently, high inhibition performance [45]. P-anisidine, therefore, has significant electron-donating power. The gap is the minimum energy needed to excite an electron in a mol-

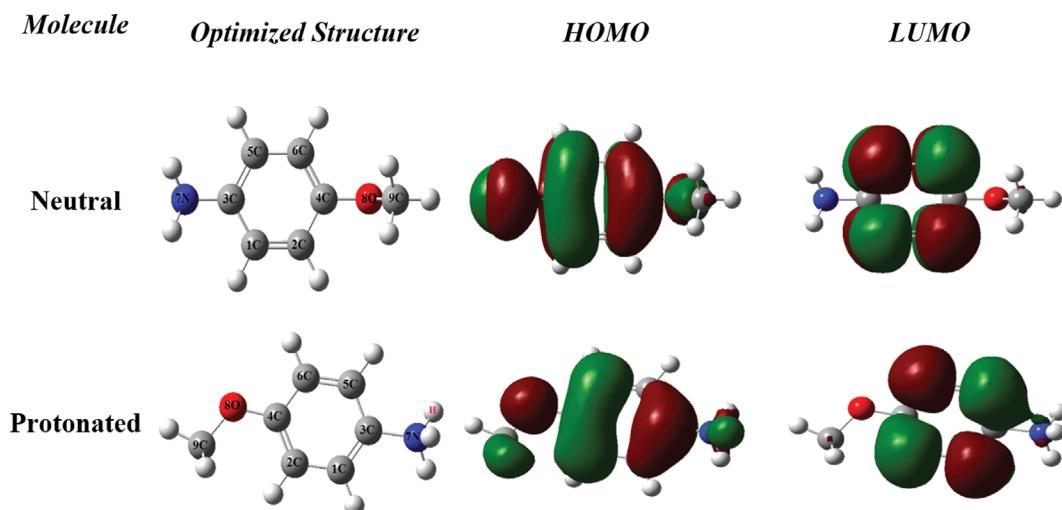


Fig. 11. Optimized structures, LUMO, and HOMO density distributions of the neutral and protonated form of P-anisidine molecule.

ecule. A low value of ΔE results in a high inhibitory efficacy. When ΔE reduces, the inhibitor reactivity vis-à-vis the metal surface augments [46].

The dipole moment is a description of the polarity of molecules [47]. It describes the distribution of electricity in a molecule and is one of the materials used to simplify the molecular structure. However, there is no consensus on the relationship between dipole moment and corrosion inhibition efficiency [48,49]. The high dipole moment is thought to result in high attenuation performance [50], and the table shows the significance of this measurement for the protonated molecule compared to the average shape, which reveals another except that protonation affects the global descriptor of reactivity. The small value of $\Delta N_{110} < 3,6$ according to Lukovits's study, indicates the enhanced ability to donate an electron to the steel surface, which can decrease the corrosion rate of the studied metal for the P-anisidine structure. Furthermore, the small value obtained for softness and the high one for hardness confirm the reactivity explained by the P-anisidine molecule.

A comparison of these results with what we obtained by studying the inhibitory power of another anisole derivative, Trans anethole, shows that the inhibitory power of this molecule remains higher by the introduction of a propene group, which is characterized by the reactivity of the double bond and which leads to an increasing value of E_{HOMO} and a corresponding decrease in the values of E_{LUMO} and ΔE_{gap} compared to P-anisidine, but in general, both derivatives are better inhibitors with an efficiency exceeding 90% at 298 K.

7-2. Location of Active Centers

The inhibitory molecule usually gives its electrons to the metal surface and also accepts electrons from the surface of the metal. It is therefore reasonable to examine the active sites of the inhibitor molecule. To do this, we calculated the Fukui indices, which are used to analyze the local reactivity as well as the nucleophilic and electrophilic behaviors of the inhibitor studied [51] (Fig. 12).

Examination of the calculations presented in Fig. 12 allows us to note that for P-anisidine, the atoms (2C, 5C, 6C, 1C) are the sites most susceptible to nucleophilic attack because these atoms have the most f_k^+ . On the other hand, the atom (4C) and the heteroat-

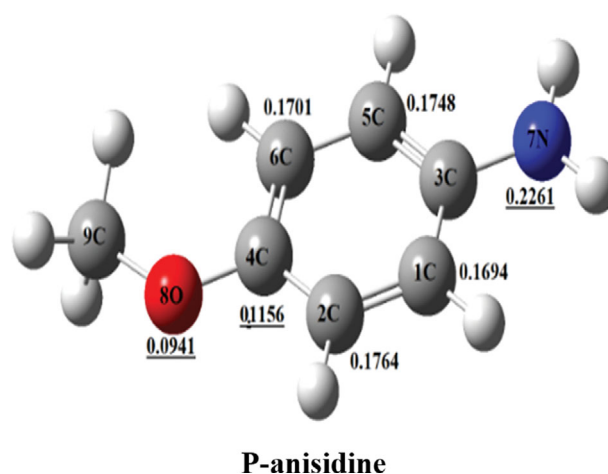


Fig. 12. Fukui function in the neutral form: f_k^+ : normal and f_k^- : underlined.

oms (7N, 8O) are the preferred sites for an electrophilic attack, especially for the atom 7N, which presents the greatest value of f_k^- , which would attribute to this site an important adsorption power on the metal surface.

7-3. Molecular Dynamic Simulations

It is well known that molecular dynamic simulation is an interesting method to establish the adsorption of the molecular structure onto the metal surface used [52]. In this case, MD simulations were performed to investigate the interfacial interactions that happen between the P-anisidine derivative and the mild steel surface, at different temperatures of 298 K and 328 K. Moreover, to approach the experimental conditions, the solvent that affects the protonation process of the studied inhibitor was considered [53,54]: The temperature, as well as the various energy type (potential, kinetic, non-bond, and total), as illustrated in Fig. 13. Furthermore, the adsorption energy values (E_{ads}) of P-anisidine inhibitor for neutral and protonated forms are calculated and regrouped in Table 7.

First, it was observed that the studied system showed an equi-

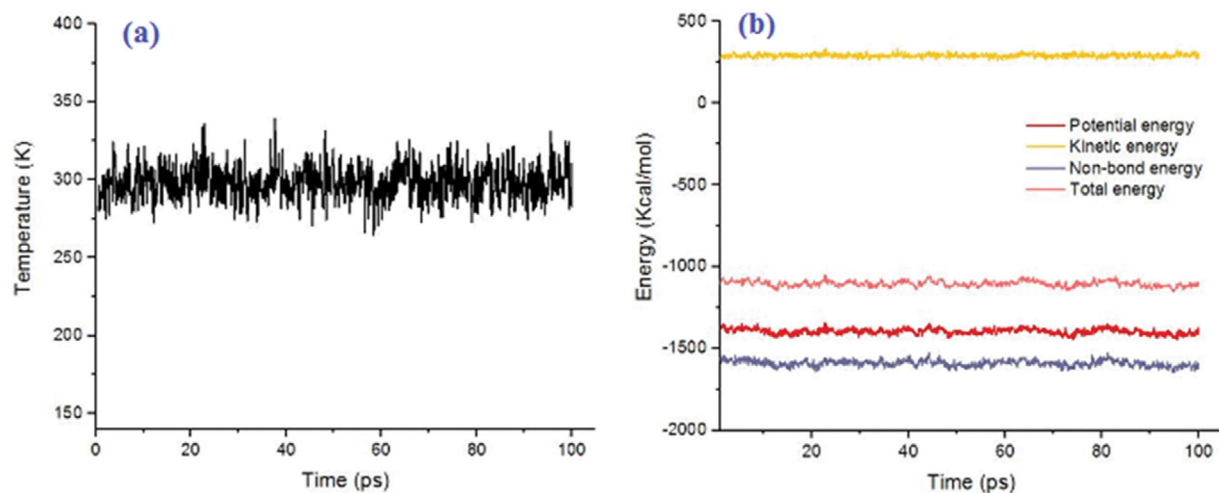


Fig. 13. (a) Temperature and (b) energy records of P-anisidine inhibitor/metal system throughout the molecular dynamic calculations.

Table 7. Adsorption energy (in Kcal mol⁻¹) for neutral and protonated P-anisidine inhibitor forms under solvation conditions at 298 and 328 K

Inhibitor form	E_{ads}	
	298 K	328 K
P-anisidine -H	-171.237	-164.855
P-anisidine	-89.247	-94.865

librium at the end of the simulation operation, which confirms the confidence of energies obtained. As we can observe from the presented values, the negative values of the obtained energies indicate the spontaneity reaction of the adsorption process of the P-anisidine molecule onto the surface [55]. On the other hand, by comparing E_{ads} of neutral and protonated inhibitor forms, we can observe

that the adsorption energy $E_{ads}(P\text{-anisidine}) > E_{ads}(P\text{-anisidine-H})$, which confirms the great ability of P-anisidine-H (protonated form) molecule to adsorb on the plan (110) of the iron metal surface. Also, this priority was detected at 298 K as well as at 328 K. On the other hand, based on the protonated form of the P-anisidine molecule, the adsorption energy at the temperature of 298 K is higher than that obtained at 328 K, confirming therefore the results obtained experimentally [56]. From the above discussion, it can be concluded that P-anisidine in the protonated form is mainly responsible for the inhibition performance behavior compared to the neutral one [57].

Additionally, Fig. 14 presents the equilibrium adsorption configuration for P-anisidine in various forms. According to the geometric aspect obtained, P-anisidine and its protonated form are placed close to the iron surface. This observation confirms the high tendency of P-anisidine structure to relate with the studied surface

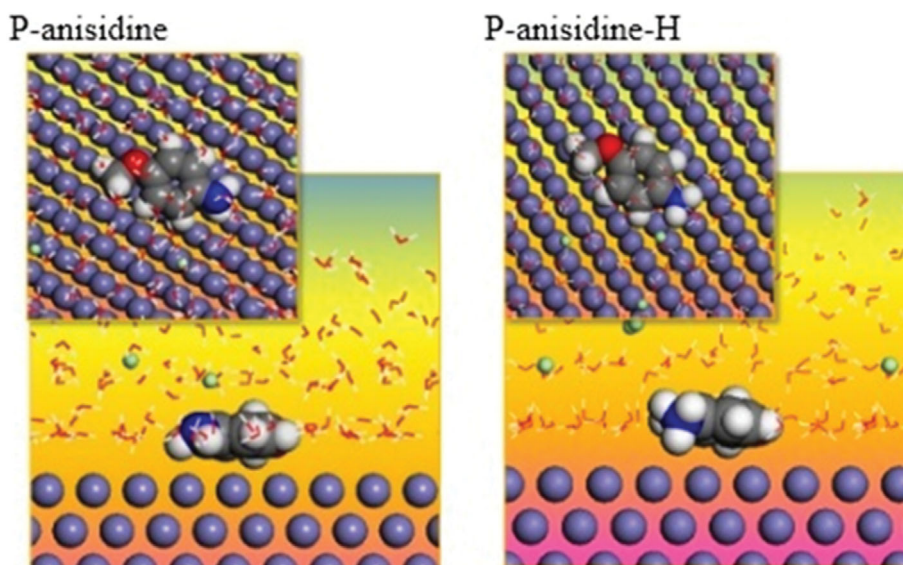
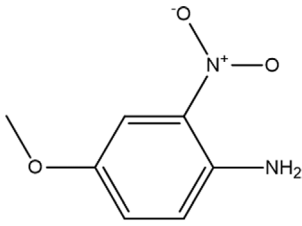
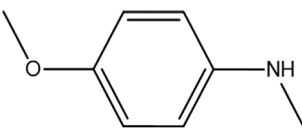
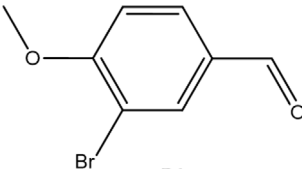


Fig. 14. Adsorption mode of neutral and protonated P-anisidine forms onto Fe(110) surface.

Table 8. Previous inhibitors as corrosion inhibitor

Inhibitors	Metal & electrolyte	Inhibitors Conc.	Isotherm	Inhibition efficiency		Ref.
				IE _{EIS}	IE _{PDP}	
	1 M HCl/ mildsteel	10 ⁻³ M	Langmuir	86.1	86.5	[60]
				82.7	82.8	
				81.9	82.6	

by strong bonds than be solvate in solution [58]. Also, the parallel adsorption mode observed led us to report that the studied structure covered a large area of the metal surface, which led to high inhibition performance [59]. From the energetic and geometric analysis, it can be concluded that the interfacial interactions that happened between P-anisidine and the steel surface showed a great correlation with the experimental part covering a large surface area making, therefore, a strong film inhibitor, i.e., making a barrier that can prevent the mild steel dissolution.

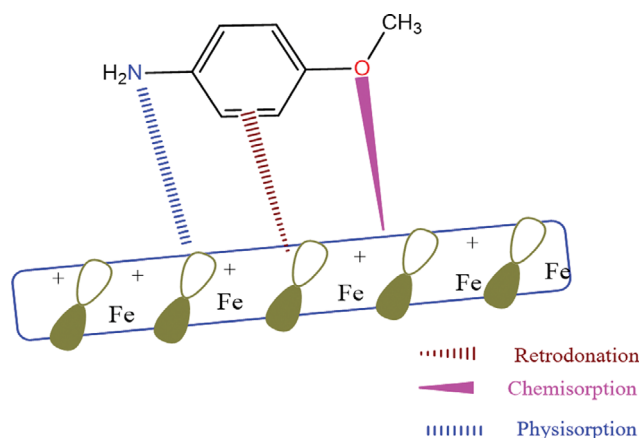
8. A Comparative Study with the Previous Paper

Recently, anisidine molecules were applied as corrosion inhibitors detecting an elevated inhibition process. The inhibition performance of the P-anisidine compound was compared to the above molecules that were published recently. The parameters, like molecule structures, electrolyte medium, maximum concentration, metal, isotherm, and their inhibition efficiencies obtained through the various experimental techniques, are summarized in Table 8.

Compared with the latest paper on anisoles derivatives [60], it is clear that the corrosion inhibition of the studied derivative with the percentage of 80.8% is based on the impedance analysis. This percentage is less than 86.5% obtained for P1 and 82.6% obtained for P2, which has amino substitution in the para site of the benzene ring. Moreover, at these molecules' derivatives can be adsorbed into the steel surface via Langmuir isotherm, making a monolayer barrier.

9. Inhibition Mechanism of P-anisidine

The results of the experimental and theoretical approach to the P-anisidine molecule indicate that the interaction between this material and the metal surface occurs during immersion in hydrochloric acid (Fig. 15). This presentation shows that P-anisidine can be

**Fig. 15. Proposed inhibition mechanism of P-anisidine.**

adsorbed on the steel surface through various interactions. First, the protonated nitrogen atom in the amino motif can be physically adsorbed with the chloride anion Cl^- . In addition, these interactions can be chemical and create interactions by exchanging their electron pairs with Fe vacant d-orbital, similar to interference with an oxygen atom and steel surface. Such interference protects the metal from extreme damage. In addition, donor interaction of π -electron clouds around the aromatic ring and the location of ionized atoms indicates that the molecule in the study formed a protective metal layer. In addition, the parallel adsorption of P-anisidine covers a large area, which explains the development of a protective layer that prevents mild steel from exploding during the corrosion process and has a high anti-corrosion ability.

CONCLUSION

The P-anisidine molecule has shown its effectiveness as essentially mixed inhibitor that acts on cathodic and anodic kinetics at the same time. Its inhibitory power increases and exceeds 81% for a concentration of 10^{-3} M. The study as a function of temperature has shown that any increase in this parameter leads to a decrease in inefficiency. From the electrochemical, thermodynamic, and surface analysis results, the mechanism of P-anisidine takes the place of a pure activation mechanism by creating a protective barrier on the steel surface resulting from the adsorption process of the inhibitor, which obeys the Langmuir isotherm and which takes place by the formation of electrostatic bonds between the molecule and the vacant "d" orbital of the steel surface. Quantum study and dynamic simulation have shown that the interfacial interaction between P-anisidine and the steel surface shows a great correlation with the experimental part covering a large surface area making a barrier film to prevent the mild steel.

ACKNOWLEDGEMENTS

This work is supported by the Korean National Research Foundation's (NRF) research program, which is funded by the Ministry of Education (2020R1I1A3052258). This work was also supported by the Technology Development Program (S3060516) funded by the Ministry of SMEs and Startups (MSS, Korea) in 2021, and the Engineering Laboratory of Organometallic, Molecular Materials, and Environment, Faculty of Sciences, Dhar El Mahraz, Sidi Mohamed Ben Abdellah University.

AUTHORS' CONTRIBUTION

Asmae Bouoidina and Rajesh Haldhar equally contributed to this work.

CONFLICTS OF INTEREST

The authors declare no conflict of interest.

REFERENCES

1. R. Haldhar, S. C. Kim, D. Prasad, M. A. Bedair, I. Bahadur, S. Kaya, O. Dagdag and L. Guo, *J. Mol. Struct.*, **1242**, 130822 (2021).
2. R. Salim, E. Ech-chihbi, H. Oudda, F. El-hajjaji, M. Taleb and S. Jodeh, *J. Bio-Tribo-Corros.*, **13**, 5 (2019).
3. N. Arrousse, E. Mabrouk, R. Salim, K. I. Alaoui, F. El-hajjaji, Z. Rais, M. Taleb and B. Hammouti, *Mater. Today: Proc.*, **27**, 3184 (2020).
4. R. Haldhar and D. Prasad, *J. Bio-Tribo-Corros.*, **6**, 48 (2020).
5. F. El-hajjaji, F. Abridgach, O. Hamed, A. R. Hasan, M. Taleb, S. Jodeh, E. Rodriguez-Castellon, M. V.M. Yuso and M. Algarra, *Coatings*, **8**, 330 (2018).
6. R. Haldhar, D. Prasad, I. Bahadur, O. Dagdag and A. Berisha, *J. Mol. Liq.*, **323**, 114958 (2021).
7. R. Haldhar, D. Prasad, I. Bahadur, O. Dagdag, S. Kaya, D. K. Verma and S. C. Kim, *J. Mol. Liq.*, **335**, 116184 (2021).
8. R. Haldhar, D. Prasad, D. Kamboj, S. Kaya, O. Dagdag and L. Guo, *Appl. Sci.*, **3**, 25 (2021).
9. B. Butoi, A. Groza, P. Dinca, A. Balan and V. Barna, *Polymers*, **9**, 732 (2017).
10. R. Haldhar, D. Prasad, N. Mandal, F. Benhiba, I. Bahadur and O. Dagdag, *Colloids Surf. A Physicochem. Eng. Asp.*, **614**, 126211 (2021).
11. S. K. Shukla and A. Quraishi, *J. Appl. Polym. Sci.*, **124**, 5130 (2012).
12. R. Karthikaiselvi and S. Subhashini, *J. Assoc. Arab Univ. Basic Appl. Sci.*, **16**, 74 (2014).
13. Y. Ma, B. Fan, H. Liu, G. Fan, H. Hao and B. Yang, *Appl. Surf. Sci.*, **514**, 146086 (2020).
14. O. Abdellaoui, M. K. Skalli, A. Haoudi, Y. K. Rodi, A. Mazzah, N. Arrousse, M. Taleb, R. Ghibate and O. Senhaji, *Mor. J. Chem.*, **9**, 44 (2021).
15. N. Arrousse, E. Mabrouk, B. Hammouti, F. El-hajjaji, Z. Rais and M. Taleb, *Int. J. Corros. Scale Inhib.*, **9**, 661 (2020).
16. N. Arrousse, R. Salim, A. Abdellaoui, F. El-hahhaji, B. Hammouti, E. Mabrouk, W. A. Dino and M. Taleb, *J. Taiwan Inst. Chem. Eng.*, **120**, 344 (2021).
17. R. Haldhar, D. Prasad, L. T. D. Nguyen, S. Kaya, I. Bahadur, O. Dagdag and S. C. Kim, *Mater. Chem. Phys.*, **267**, 124613 (2021).
18. E. Ech-chihbi, A. Nahlé, R. Salim, F. Benhiba, A. Moussaif, F. El-hajjaji, H. Oudda, A. Guenbour, M. Taleb, I. Warad and A. Zarrouk, *J. Alloys Compd.*, **844**, 155842 (2020).
19. R. Haldhar, D. Prasad and H. Saharan, *J. Ind. Eng. Chem.*, **11**, 1 (2020).
20. H. Bourzi, R. Oukhrib, B. El-Ibrahimi, H. A. Oualid, Y. Abdellaoui, B. Balkard, S. El-Issami, M. Hilali, L. Bazzi and C. Len, *Sustainability*, **12**, 3304 (2020).
21. R. Haldhar, D. Prasad and A. Saxena, *J. Environ. Chem. Eng.*, **6**, 5230 (2018).
22. B. El-Ibrahimi, A. Jmiai, K. El-Mouaden, R. Oukhrib, A. Soumoue, S. El-Issami and L. Bazzi, *J. King Saud Univ. Sci.*, **32**, 163 (2020).
23. B. El-Ibrahimi, *Colloids Interface Sci. Commun.*, **37**, 100279 (2020).
24. A. Farhadian, S. A. Kashani, A. Rahimi, E. E. Oguzie, A. J. Parvar, S. C. Nwanonenyi, S. Y. Zadeh and M. R. Nabi, *J. Mol. Liq.*, **338**, 11660 (2021).
25. R. Haldhar, D. Prasad, A. Saxena and A. Kaur, *Eur. Phys. J. Plus*, **133**, 356 (2018).
26. S. K. Saha, A. Dutta, P. Ghosh, D. Sukul and P. Banerjee, *Phys. Chem. Chem. Phys.*, **18**, 17898 (2016).
27. P. P. Kumari, P. Shetty and S. A. Rao, *Arab. J. Chem.*, **10**, 653 (2017).
28. A. Saady, E. Ech-chihbi, F. El-hajjaji, F. Benhiba, A. Zarrouk, Y. Kandrirodi, M. Taleb, A. El-Biache and Z. Rais, *J. Appl. Electrochem.*, **51**, 245 (2021).
29. Y. Zhang, B. Tan, X. Zhang, L. Guo and S. Zhang, *J. Mol. Liq.*, **33**, 116702 (2021).
30. G. Sigircik, T. Tunc and M. Erbil, *Corros. Sci.*, **102**, 437 (2016).
31. B. Xu, W. Yang, Y. Liu, X. Yin, W. Gong and Y. Chen, *Corros. Sci.*, **78**, 260 (2014).
32. R. S. A. Hameed, M. Alfakeer and M. Abdallah, *Surf. Eng. Appl. Electrochem.*, **54**, 599 (2018).
33. N. Arrousse, R. Salim, I. B. Obot, A. Abdellai, F. El-hajjaji, E. Mabrouk and M. Taleb, *J. Mol. Liq.*, **359**, 119311 (2022).
34. A. Ghazoui, N. Benchat, F. El-hajjaji, M. Taleb, R. Rais, R. Saddik, A. Elaataoui and B. Hammouti, *J. Alloys Compd.*, **693**, 510 (2017).
35. S. A. Mrani, E. Ech-chihbi, N. Arrousse, Z. Rais, F. El-hajjaji, C. El-

- Abiad, S. Radi, J. Mabrouki, M. Taleb and S. Jodeh, *Arab. J. Sci. Eng.*, **46**, 5691 (2021).
36. Y. W. Liu, Y. Chen, X. H. Chen, Z. N. Yang and Z. Z. Hang, *J. Alloys Compd.*, **758**, 184 (2018).
37. A. Nahlé, R. Salim, F. El-hajjaji, M. R. Aouad, M. Messali, E. Ech-chihbi, B. Hammouti and M. Taleb, *RSC Adv.*, **11**, 4147 (2021).
38. M. Messali, M. Larouj, H. Lgaz, N. Rezki, F. F. Al-Blewi, M. R. Aouad, A. Chaoui, R. Salghi and M. L. Chung, *J. Mol. Struct.*, **1168**, 39 (2018).
39. N. Arrousse, R. Salim, F. Benhiba, E. H. Mabrouk, A. Abdelaoui, F. El-hajjaji, I. warad, A. Zakkrouk and M. Taleb, *J. Mol. Liq.*, **338**, 116610 (2021).
40. F. El-hajjaji, R. Salim, M. Messali, B. Hammouti, D. S. Chauhan, S. M. Almutairi and M. A. Quraishi, *J. Bio-Tribo-Corros.*, **5**, 4 (2019).
41. A. Rahimi, M. Abdouss, A. Farhadian, L. Guo and J. Neshati, *Eng. Chem. Res.*, **60**, 11030 (2020).
42. N. E. Chile, R. Haldhar, U. K. Godffrey, O. C. Chijioke, E. A. Umezuruike, O. P. Ifeoma, M. O. Oke, H. Ichou, N. Arrousse, S. C. Kim, O. Dagdag, E. E. Ebenso and M. Taleb, *Lubricants*, **10**, 1 (2022).
43. A. Saady, F. El-hajjaji, M. Taleb, K. I. Alaoui, A. El-Biache, A. Mahfoud, G. Alhouari, B. Hammouti, D. S. Chauhan and M. A. Quraishi, *Mater. Discov.*, **12**, 30 (2019).
44. P. P. Kumari, P. Shetty and S. A. Rao, *Arab. J. Chem.*, **10**, 653 (2017).
45. P. Dohare, D. S. Chauhan, A. A. Sorour and M. A. Quraishi, *Mater. Discov.*, **9**, 30 (2017).
46. A. Y. Obaid, A. A. Ganash, A. H. Qusti, S. A. Elroby and A. A. Her-mas, *Arab. J. Chem.*, **10**, S1276 (2017).
47. L. C. Murulana, A. K. Singh, S. K. Shukla, M. M. Kabanda and E. E. Ebenso, *Ind. Eng. Chem. Res.*, **51**, 13282 (2012).
48. Q. Ma, S. Qi, X. He, Y. Tang and G. Lu, *Corros. Sci.*, **129**, 91 (2017).
49. J. Lazrak, R. Salim, N. Arrousse, E. Ech-chihbi, F. El-hajjaji, M. Taleb, F. Farah and A. Ramzi, *Int. J. Corros. Scale Inhib.*, **9**, 1580 (2020).
50. O. Olasunkanmil, I. B. Obot, M. M. Kabanda and E. E. Ebenso, *J. Phys. Chem.*, **119**, 16004 (2015).
51. F. El-hajjaji, E. Ech-chihbi, N. Rezki, F. Benhiba, M. Taleb, D. S. Chauhan and M. A. Quraishi, *J. Mol. Liq.*, **314**, 113737 (2020).
52. R. Kumar, S. Chahal, S. Kumar, S. Lata, R. Salghi, S. Jodeh and H. Lgaz, *J. Mol. Liq.*, **243**, 439 (2017).
53. H. Hamani, T. Douadi, D. Daoud, M. Al-Noaimi, R. A. Rikkouh and S. Chafaa, *J. Electroanal. Chem.*, **801**, 425 (2017).
54. B. El-Ibrahimi, A. Jmiai, K. El-Mouaden, A. Baddouh, S. El-Issami, L. Bazzi and M. Hilali, *J. Mol. Struct.*, **1196**, 105 (2019).
55. Y. Qiang, S. Zhang, L. Guo, X. Zheng, B. Xiang and S. Chen, *Corros. Sci.*, **119**, 68 (2017).
56. A. Singh, K. R. Ansari, Y. Lin, M. A. Quraishi, H. Lgaz and I. M. Chung, *J. Taiwan Inst. Chem. Eng.*, **95**, 341 (2018).
57. F. El-hajjaji, R. Salim, M. Taleb, F. Benhiba, N. Rezki, D. S. Chauhan and M. A. Quraishi, *Surf. Interfaces*, **22**, 100881 (2021).
58. F. Li, M. Bai, S. A. Wei, S. Jin and W. Shen, *Ind. Eng. Chem. Res.*, **58**, 7166 (2019).
59. L. Feng, S. Zhang, Y. Qiang, S. Xu, B. Tan and S. Chen, *Mater. Chem. Phys.*, **215**, 229 (2018).